

Effects of isotope disorder on energies and lifetimes of phonons in germanium

A. Göbel, D. T. Wang, and M. Cardona

Max-Planck Institut für Festkörperforschung, Heisenbergstrasse 1, D-70569 Stuttgart, Germany

L. Pintschovius

*Forschungszentrum Karlsruhe, INFP, Postfach 3640, D-76021 Karlsruhe, Germany
and Laboratoire Léon Brillouin, C.E.-Saclay, F-91191 Gif-sur-Yvette Cedex, France*

W. Reichardt

Forschungszentrum Karlsruhe, INFP, Postfach 3640, D-76021 Karlsruhe, Germany

J. Kulda and N. M. Pyka

Institut Laue-Langevin, B.P.156, F-38042 Grenoble Cedex 9, France

K. Itoh* and E. E. Haller

University of California and Lawrence Berkeley National Laboratory, Berkeley, California 94720

(Received 17 April 1998)

The effects of isotope disorder on phonon energies and lifetimes have been measured by means of high-resolution inelastic neutron scattering on a nearly maximally disordered $^{70/76}\text{Ge}$ single crystal (mass variance $g = 1.52 \times 10^{-3}$). Two theoretical approaches have been used to understand the observed effects: calculations based on the coherent potential approximation and on large supercells, respectively. For the mass variance of our sample, the two methods lead to rather similar results that agree with the experimental data. This agreement is marginally better for the supercell calculations. Calculations performed for larger mass variances g revealed, however, that the two approaches yield significantly different results when g is larger than 3×10^{-3} . [S0163-1829(98)02938-5]

I. INTRODUCTION

The influence of the isotopic composition of semiconductors on their physical properties has received considerable attention during the last decade. Several publications¹⁻⁴ review aspects such as the influence of the isotopic composition on the lattice constant of germanium⁵⁻⁷ and of compound semiconductors^{8,9} or the changes in the renormalization of the fundamental gap due to electron-phonon coupling.⁹⁻¹² The thermal conductivity is strongly affected by isotope disorder, e.g., it is increased by a factor of ten in isotopically pure germanium with respect to that of natural germanium crystals.¹³ In certain cases, isotope substitution can be used either to discern the effects of isotope-disorder-induced phonon scattering from those stemming from the anharmonic decay of phonons,¹⁴⁻¹⁶ or to tune the effect of anharmonic decay channels.¹⁷ Isotopically controlled multilayer structures of Ge, GaAs, GaP, and Si have been used successfully for the study of self-diffusion.¹⁸

In this paper, we investigate the effects of the isotopic composition on the energies and lifetimes of phonons in Ge. Isotopic mass fluctuations in elemental semiconductors represent a particularly simple form of disorder that involves only mass fluctuations but no significant structural or force constant disorder. Phonons are thus well suited for the theoretical and experimental study of isotope disorder effects. We note that the statement “no force constant disorder” is not invalidated in any significant way by the above-cited findings that the lattice constant and the electronic properties

of Ge do in fact slightly depend on the isotopic composition; these effects are so small that their influence can be totally neglected in the framework of the present investigation. Therefore, disorder-induced effects on the energies and lifetimes of phonons appear as an ideal testing ground for theories widely used for disordered systems like, e.g., the coherent potential approximation (CPA). Germanium is especially well suited for such a study for several reasons: (i) the range of masses covered by its stable isotopes is rather large (i.e., from 70 to 76 amu), (ii) it can be grown as single crystals with a high degree of perfection, and (iii) anharmonic effects are relatively small, leading to long lifetimes in the absence of isotope disorder.

However, earlier efforts to study isotope-disorder-induced effects on phonons remained unsatisfactory for a number of reasons. To begin with, high precision (first-order) Raman measurements are confined to optical phonons at the center of the Brillouin zone. Due to the vanishing one-phonon density of states at the Γ point optical phonon frequency,¹⁹ the disorder effect on the linewidth is very small¹ and has to compete with the anharmonic broadening and also line asymmetry effects due to the finite penetration depth of the laser light.¹⁴⁻¹⁶ More indirect measurements of the phonon energies and lifetimes at other high symmetry points of the Brillouin zone such as infrared absorption, photoluminescence or second-order Raman scattering suffer from inherently poor experimental resolution and/or additional contributions to the line shape that cannot be accurately disentangled.²⁰ Inelastic neutron scattering is, in principle,

TABLE I. Isotope masses, isotopic composition, average masses \bar{m} , and mass variance parameter g of natural Ge as well as the samples used in the experiment.

	[amu]	nat. Ge	^{70}Ge	$^{70/76}\text{Ge}$
^{70}Ge	69.924249	20.5%	> 99.99%	42.7%
^{72}Ge	71.922079	27.4%		2.1%
^{73}Ge	72.923462	7.8%		< 0.1%
^{74}Ge	73.921177	36.5%		7.2%
^{76}Ge	75.921401	7.8%		48.0%
\bar{m} [amu]		72.6323	69.9242	73.1326
g		0.587×10^{-3}	$< 1.0 \times 10^{-7}$	1.532×10^{-3}

the method of choice to investigate the phonon frequencies and linewidths throughout the whole Brillouin zone. However, the experimental resolution achieved in earlier neutron measurements was rather coarse compared with optical methods and only a moderately disordered crystal of natural isotopic composition was available to compare with an isotopically pure one, so that the error margins remained large.²⁰

On the theoretical side, the predictions of the CPA and a self-consistent Born approximation (SCBA) appeared to differ, even qualitatively.²⁰ This is surprising in so far as the disorder is rather weak, so that both perturbative approaches should give similar results. Indeed, later results of CPA calculations on the effects of isotope disorder in α tin¹⁵ closely resemble those of SCBA calculations for Ge. The combined deficiencies on the experimental as well as the theoretical side stimulated the present investigation.

In this work we present a comprehensive study of the effect of isotope disorder on the phonon energies and lifetimes in germanium. The experimental situation was improved with respect to previous work in two respects: We grew a Ge single crystal with an isotope disorder close to the maximum achievable (that would be $^{70}\text{Ge}_{0.5}^{76}\text{Ge}_{0.5}$), and we used experimental setups with a considerably improved energy resolution. This enabled us to detect disorder-induced line shifts and line broadenings with sufficient accuracy to check theoretical predictions quantitatively, at least within the energy range of the optical phonons. On the theoretical side, we have not only checked and corrected previous CPA results,²⁰ but also employed a new technique, i.e., the simulation of isotope disorder using large supercells (SC's). The comparison of both approaches with our experimental data is based on the theoretically predicted spectral density function, which may be strongly asymmetric, properly convoluted with the experimental resolution. We point out that the usual approximation of the disorder-induced line shape as a Lorentzian contribution to the inverse lifetime may easily lead to poor agreement between theory and experiment. Furthermore, we have extended the calculations to mass variances larger than those obtainable with Ge.

The paper is organized as follows: In Sec. II we discuss the experimental technique and describe the samples. The experimental data are presented in Sec. III, while Sec. IV comprises a discussion of the details of the supercell calculations and those of the CPA. Both approaches are compared in detail to each other in Sec. V and to our data in Sec. VI. Earlier results are discussed in Sec. VII, whereas Sec. VIII is devoted to the conclusions.

II. EXPERIMENT

A. Samples

The undoped Ge samples we have used are a nearly isotopically pure single crystal (^{70}Ge) and a highly isotopically disordered one ($^{70/76}\text{Ge}$). Both samples are approximately cylinders about 1 cm long, with a diameter of about 0.9 cm, and have a similar crystal orientation. The mosaic spread of both samples was found to be smaller than 0.1° . The mass variance parameter g , which characterizes the isotopic mass fluctuations in a monoatomic sample, is defined as

$$g = \sum c_i \left[\frac{\bar{m} - m_i}{\bar{m}} \right]^2,$$

where c_i denotes the concentration of the isotope with mass m_i . For convenience, we list the average masses \bar{m} , and the isotopic composition of our samples and that of natural germanium together with g in Table I. Our $^{70/76}\text{Ge}$ sample is nearly maximally disordered, i.e., the mass variance parameter g is close to the maximum value of 1.7×10^{-3} obtainable with Ge for a perfect ‘‘fifty-fifty’’ alloy ($^{70}\text{Ge}_{0.5}^{76}\text{Ge}_{0.5}$).

Within the harmonic approximation ($\nu \sim \bar{m}^{-1/2}$) we expect the phonon frequencies of the ^{70}Ge sample to be by a factor of 1.0227 larger than those of the $^{70/76}\text{Ge}$ crystal.

B. Neutron scattering

The investigation of the optical phonons by inelastic neutron scattering was carried out on the 2T-triple axis spectrometer located at a thermal beam tube of the ORPHEE reactor at the Laboratoire Léon Brillouin, Saclay. Horizontally and vertically focusing Cu-220 and PG-002 crystals were used as monochromator and analyzer, respectively. Details of the instrument have been described in Ref. 21.

The final energy was kept fixed at $E_F = 3.55$ THz or $E_F = 3.25$ THz, which allowed us the use of a PG filter in the scattered beam to suppress second-order contaminations. The energy resolution of our setup was between 8.7 and 13 cm^{-1} [(full width at half maximum) FWHM], depending on the phonon energy (250 to 300 cm^{-1}) and the focusing conditions.

In order to keep errors associated with an off-center position of the samples to a minimum, the samples were carefully aligned with the help of a laser beam. Furthermore, all phonon measurements were repeated after turning the sample by 180° and the two energy values obtained in this way were

averaged. By this procedure, we believe to have reduced any errors resulting from potential off-center positions of the samples to a negligible size. A further check of the alignment dependence was performed by repeating a large part of the measurements after a second alignment for both samples. The data obtained in the two runs agreed well with each other. Averaging the values of the two runs leads to the final results. To a first approximation disorder-induced effects should be proportional to the product of the mass variance, the square of the frequency and the one-phonon density of states (DOS).²² Hence, it is important to cover a frequency range in the experiment where the DOS varies from very small to large and again to vanishingly small, i.e., from about 250–300 cm^{-1} .²³

We originally intended to focus our efforts on the $\Delta'_2(O)$ branch,²⁴ because it would have given us the opportunity to study the energy dependence of the disorder-induced line shifts and linewidths on a single branch for the whole energy range of interest under very good experimental conditions (large momentum transfers, favorable selection rules, good focusing conditions). However, we soon became aware of the fact that $\Delta'_2(O)$ phonons show a very appreciable broadening in a certain energy range, even in the absence of isotope disorder, which is probably due to anharmonic decay. This makes it difficult to extract the additional line broadening associated with isotope disorder in a quantitative way. As a consequence, we resorted to the investigation of two other branches, i.e., the $\Delta_5(O)$ and the $\Sigma_3(O)$ branches, along which the anharmonic broadening was found to be much less severe, although not always negligible. Unfortunately, this advantage had to be paid for by less favorable selection rules, so that the observed intensities sometimes contained non-negligible contributions from another branch. The way in which we dealt with this problem will be described in Sec. III A. The final measurements were carried out around the (2,4,4)-reciprocal lattice points, i.e., going from $Q=(2,4,4)$ to $Q=(1,4,4)$ or from $Q=(2,4,4)$ to $Q=(2, 3.5, 3.5)$ for the measurements of the $\Delta_5(O)$ and the $\Sigma_3(O)$ branches, respectively. All measurements were performed at ambient conditions for the sake of a precise positioning of the samples.

The investigation of the acoustic phonons was performed on the IN20 spectrometer at the Institut Laue-Langevin, Grenoble. Isotope disorder effects similar to those expected for the optical phonons are predicted for the acoustic ones in the frequency range from 50 to 120 cm^{-1} , where the DOS exhibits a marked peak stemming from the flat transverse acoustic branches. Although the magnitude of the disorder-induced shift and broadening is expected to be about 10 times less than in the optical range, it might be possible to observe them if a suitable focusing geometry is chosen in reciprocal space, for which the inclination of the resolution ellipsoid matches the slope of the dispersion surface. Particularly favorable conditions have been achieved by using an elastically bent perfect Si-111 monochromator and analyzer with a rather weak curvature.²⁵

The present measurements were carried out in three adjacent frequency ranges of 24–34, 39–67, and 67–98 cm^{-1} in the (4,2,2), (0,4,4), and (4,0,0) Brillouin zones corresponding to the TA phonon branches $\Lambda_3(A)$, $\Delta_5(A)$, $\Sigma_3(A)$, respectively.²⁴ All the scans were performed in the E

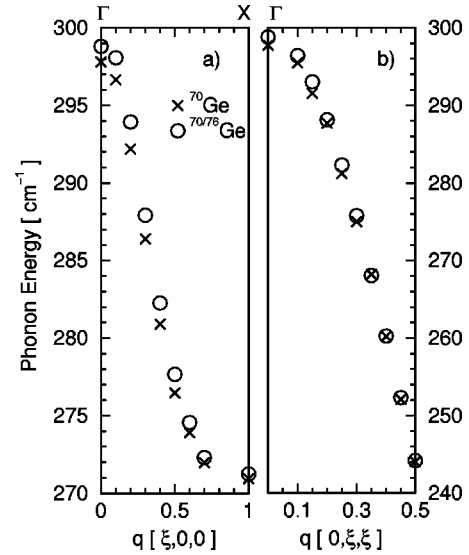


FIG. 1. Phonon frequencies measured using inelastic neutron scattering at room temperature. The data obtained for the ^{70}Ge (\times symbol) have been divided by 1.0227 to correct for the trivial mass dependence. (a) $\Delta_5(O)$, (b) $\Sigma_3(O)$; Note also the different scales.

=constant mode in order to minimize mechanical positioning errors of the spectrometer. At each energy transfer, both symmetry related scans at \vec{Q} and $-\vec{Q}$ were performed. The two peak positions did not differ by more than 5×10^{-4} reciprocal lattice units (r.l.u.) and their mean was used in the further evaluation. The consistency of the data is further supported by the fact that no significant difference was found between the results obtained in two independent experiments separated by one year!

III. EXPERIMENTAL RESULTS

A. Optical branches

The phonon energies ν obtained along the high symmetry directions Δ and Σ , extracted by fitting Gaussians to the measured spectra, are shown in Fig. 1 for both crystals. We have adjusted the frequency of the nearly isotopically pure ^{70}Ge crystal for the difference in the average mass of the two crystals, i.e., we have divided the measured frequencies by 1.0227. Therefore, within the harmonic approximation together with the virtual crystal approximation (VCA), the phonon frequencies of both crystals should coincide and we ascribe the remaining differences $\delta\nu = \nu_{\text{disordered}} - \nu_{\text{ordered}}$ in the phonon energies shown in Fig. 1 to disorder-induced scattering. The energies ν_{corr} (corrected for the harmonic mass dependence) obtained for the phonons of the ^{70}Ge sample are listed in Table II together with the disorder-induced shift $\delta\nu$ observed for the $^{70/76}\text{Ge}$ sample.

The linewidths Γ (FWHM) that we obtained from a fit of a Gaussian to the measured spectra are shown in Fig. 2. For the isotopically pure sample, there are three contributions to the linewidth: An instrumental contribution due to the finite resolution in energy and momentum transfer, a contribution due to anharmonic broadening and a contribution associated with the nonvanishing scattering cross section of branches, other than those giving the main contribution [which was $\Delta'_2(O)$ for the measurements along the (100) and $\Sigma_1(O)$

TABLE II. The phonon frequencies of the isotopically modified Ge crystals listed here were measured at the reduced wave vectors \vec{q} at room temperature. ν_{corr} denotes the phonon frequency measured for the ^{70}Ge crystal after division by 1.0227 to correct for the trivial mass dependence $\sim m^{-1/2}$ and thus allow comparison with the $^{70/76}\text{Ge}$. $\delta\nu$ is the difference between the frequency found for the isotopically disordered and the corrected frequency of the isotopically ordered sample: [$\delta\nu = \nu(^{70/76}\text{Ge}) - \nu_{\text{corr}}$]. $\delta\Gamma$ is the difference in the phonon linewidths (FWHM) obtained for the isotopically disordered and pure sample. $\delta\Gamma$ is gained from a comparison of the observed linewidths with the spectrometer resolution as described in Sec. III A and Fig. 2. Errors in $\delta\nu$ and $\delta\Gamma$ are smaller than 0.4 cm^{-1} .

$\vec{q} = (q_x, q_y, q_z)$	$\nu_{\text{corr}} [\text{cm}^{-1}]$	$\delta\nu(\Sigma_3(O)) [\text{cm}^{-1}]$	$\delta\Gamma(\Sigma_3(O)) [\text{cm}^{-1}]$
(.50, .50, 0)	244.1	0.18	0
(.45, .45, 0)	252.1	0.26	0
(.40, .40, 0)	260.2	0.08	0
(.35, .35, 0)	268.2	0.01	1.41
(.30, .30, 0)	275.0	0.77	2.34
(.25, .25, 0)	281.3	1.07	2.14
(.20, .20, 0)	287.7	0.46	1.22
(.15, .15, 0)	291.6	1.51	1.44
(.10, .10, 0)	295.5	0.96	0
$\vec{q} = (q_x, q_y, q_z)$	$\nu_{\text{corr}} [\text{cm}^{-1}]$	$\delta\nu(\Delta_5(O)) [\text{cm}^{-1}]$	$\delta\Gamma(\Delta_5(O)) [\text{cm}^{-1}]$
(1.0, 0, 0) ^a	270.9	0.32	1.73
(0.7, 0, 0)	272.0	0.31	1.73
(0.6, 0, 0)	273.9	0.66	2.05
(0.5, 0, 0)	276.5	1.23	2.22
(0.4, 0, 0)	280.9	1.41	1.36
(0.3, 0, 0)	286.4	1.56	1.19
(0.2, 0, 0)	292.2	1.77	0.91
(0.1, 0, 0)	296.6	1.47	0
(0.0, 0, 0)	297.8	1.03	0

^aThis row denotes the average of measurements at several \vec{q} points: $\vec{q} = (1,0,0), (.9,0,0), (.8,0,0)$. A comparison of these spectra is shown in Fig. 3.

along the (011) direction]. Contributions from $\Delta_2'(O)$ phonons did not lead to noticeable distortions of the $\Delta_5(O)$ phonon peaks. For this reason, we fitted all these lines with a single Gaussian. On the other hand, some of the $\Sigma_3(O)$ phonon lines were obviously distorted by contributions from $\Sigma_1(O)$ phonons. These peaks were fitted with two Gaussians, whereby the energy separation of the two peaks was fixed according to the data of Nilsson and Nelin,²⁴ their relative amplitude according to the calculated scattering cross sections, and the width taken to be the same as that of the main line. When the contribution of the $\Sigma_1(O)$ phonons was subtracted from the raw data, the corrected data points were well described by a single Gaussian.

The scans were simulated on the basis of the calculated four-dimensional resolution in energy and momentum transfer as well as the lattice dynamics of Ge modeled by a valence-force model. The instrumental parameters entering into the resolution calculation were slightly adjusted so as to reproduce the observed linewidth of about 13 cm^{-1} at the zone center Γ . The solid curves in Fig. 2 correspond to the expected linewidths as a function of reduced wave vector. For the ^{70}Ge sample the observed linewidths for the $\Delta_5(O)$ phonons, which have a transverse optic character, are well described by the solid line, whereas the corresponding linewidths of the $\Sigma_3(O)$ phonons are systematically larger for $q > 0.1$ r.l.u. Presumably, the excess linewidth is due to a

wave-vector-dependent contribution from the anharmonicity. Since we cannot model this additional anharmonic broadening, we deduced the dashed line from the data as the smoothed variation of the linewidth. Following this procedure, we define the additional broadening arising from isotope disorder as the difference between the linewidths obtained from fits of Gaussians to the experimental spectra [$\delta\Gamma = \Gamma(^{70/76}\text{Ge}) - \Gamma(^{70}\text{Ge})$]. In this manner, we are able to extract the disorder-induced broadening with an overall accuracy of about 0.4 cm^{-1} . The disorder-induced broadenings $\delta\Gamma$ are listed in Table II. The choice of the above procedure does not imply that the disorder-induced broadening has a Gaussian line shape. On the contrary, we will find in Sec. V that the disorder-broadened phonons (without experimental broadening) have line shapes which can vary from being Gaussian-like to being Lorentzian-like, depending on the length of the baseline obtained in the measurement. In addition to these, and for certain energy regimes, we also find very asymmetric profiles. We thus emphasize, that this procedure is solely applied, so that we obtain a number for (the size of) the disorder-induced broadening from the data in a manner that can be consistently applied to the theoretical results. Furthermore, it is important to notice that we have included the anharmonic contribution to the phonon linewidth in the experimental resolution and consequently slightly overestimated the latter. Although the intrinsic pho-

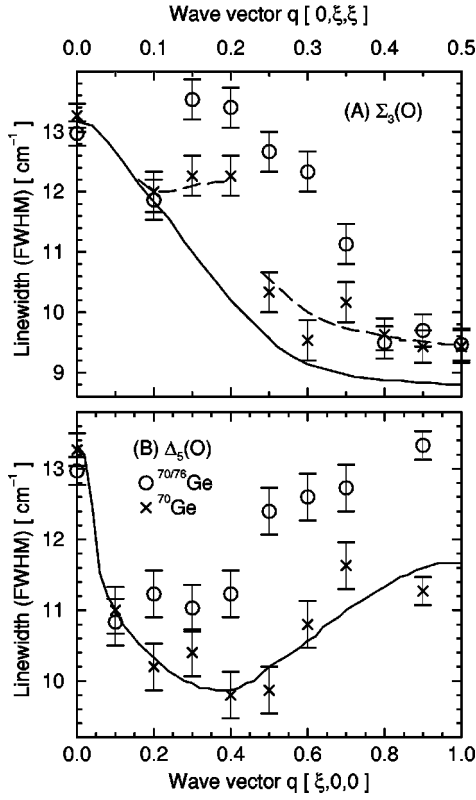


FIG. 2. Phonon linewidths obtained from a fit of a Gaussian profile for the isotopically ordered (\times symbol) and for the disordered (\circ symbol) germanium samples along two optical branches. The solid lines represent the (ω, \vec{q}) dependence of the experimental resolution. The dashed lines are a smoothed variation of the linewidths observed on the $\Sigma_3(O)$ branch of the ^{70}Ge sample. The jump at $\vec{q}=(0,0,22,0,22)$ is caused by the change in the fitting strategy from one Gaussian to two Gaussians needed to take contributions from other branches into account.

non linewidth in an ordered germanium crystal of about 2 cm^{-1} (Ref. 26) at room temperature is not negligible, its mass dependence is already small at low temperature¹⁶ and becomes even smaller with increasing temperature. The same holds for the mass dependence of the anharmonic shift.^{15,16} As a result, we can safely ignore these effects since they are much smaller than the disorder-induced shift and broadening. Finally, we point out that in evaluating the disorder-induced linewidth we made allowance for the energy dependence of the instrumental resolution, thus taking into consideration the fact that the phonon energies of the two samples differed by 2.27%.

Phonon peaks at two different \vec{q} points and frequency regimes are shown in Fig. 3. While the disorder-induced broadening in Fig. 3(a) is practically zero, a disorder-induced shift is clearly observed at this frequency ($\sim 298 \text{ cm}^{-1}$). In contrast, the phonons in the vicinity of the X point ($\sim 272 \text{ cm}^{-1}$) exhibit a substantial broadening for the disordered $^{70/76}\text{Ge}$ sample. This phonon peak is shown in Fig. 3(b) compared with the corresponding phonon of the isotopically pure sample. The spectrum shows evidence for a Voigt profile (i.e., a convolution of a Lorentzian with a Gaussian²⁷); we will discuss in how far the assumption of a symmetric Lorentzian disorder-induced broadening is justified in Sec. VI.

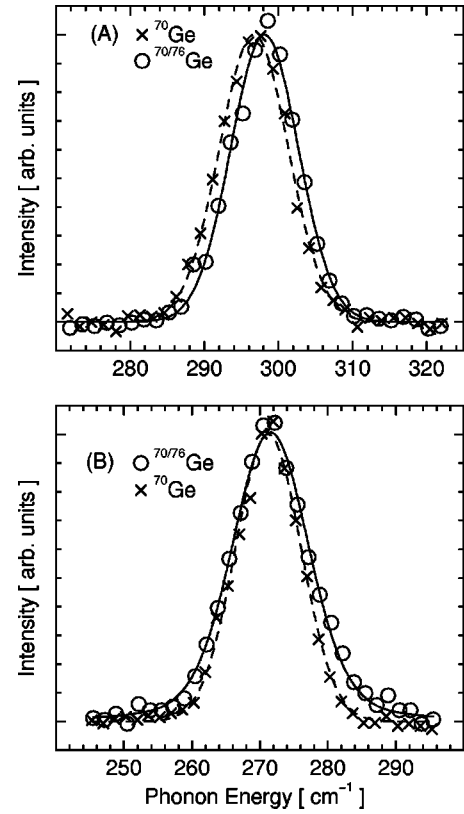


FIG. 3. Averaged and normalized phonon spectra obtained at room temperature from the $\Delta_5(O)$ branch. The energy of the ^{70}Ge phonon was divided by 1.0227, so that the remaining difference in energy is disorder-induced. (A) Spectra were obtained at $\vec{q}=(0.1,0,0)$; $\delta\nu(\Delta_5(O))=1.47 \text{ cm}^{-1}$. At this frequency ($\sim 298 \text{ cm}^{-1}$) the disorder-induced line broadening is negligible. (B) For both samples the spectra are the average obtained at the \vec{q} points: $(1.0,0,0)$, $(0.9,0,0)$, and $(0.8,0,0)$, which are observed at the same energy. In the case of the isotopically pure ^{70}Ge sample (\times symbol) we used a Gaussian to fit the data [dashed line, $\Gamma=11.4 \text{ cm}^{-1}$ (FWHM)]. In the case of the isotopic alloy $^{70/76}\text{Ge}$ (\circ symbol) a Voigt profile was used (full line), where the Gaussian contribution to the linewidth was set to 11.4 cm^{-1} , corresponding to the resolution obtained for the ^{70}Ge sample. The additional Lorentzian-like broadening was found to be $\Gamma_{\text{Lor}}=3.5 \text{ cm}^{-1}$ (FWHM).

B. Acoustic branches

We have performed neutron scattering measurements of acoustic phonons along the $\Sigma_3(A)$, $\Delta_5(A)$, and $\Lambda_3(A)$ branches. The ideal focusing conditions achieved using elastically bent perfect Si crystals as monochromator and analyzer allowed us to observe very narrow phonon lines for which the number of data points on the line was limited by the minimum step size of the instrument drives. In Fig. 4 we show phonon profiles that were obtained at an energy transfer of $\Delta E=80 \text{ cm}^{-1}$ along the $\Sigma_3(A)$ branch. In order to understand the origin of the asymmetric shapes of the scanned profiles we have calculated a 4D convolution of a model phonon dispersion for germanium with the instrumental resolution ellipsoid using the ResTrax program.²⁸ While these calculations reproduced rather closely the shapes of the observed profiles and their evolution with energy transfer, they were not well suited for direct data fitting. Therefore,

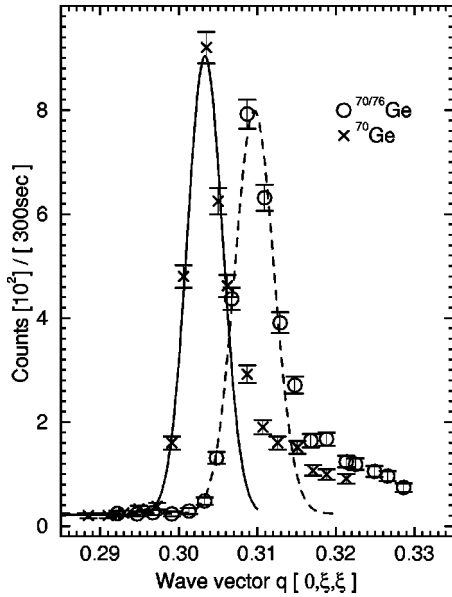


FIG. 4. Phonon lines obtained in constant energy scans ($\Delta E = 80 \text{ cm}^{-1}$). The data, which correspond to $\Sigma_3(A)$ phonons, are not corrected for the harmonic mass dependence. The solid and the dashed line represent fits of Gaussians to the main part of the phonon peaks obtained for the ^{70}Ge and $^{70/76}\text{Ge}$ samples, respectively.

we have fitted the main part of the phonon lines with two Gaussians (compare Fig. 4). The total width of about $5.6(3) \times 10^{-3}$ r.l.u. observed for the isotopically pure sample, corresponds to $1.26(7) \text{ cm}^{-1}$ on the energy scale. This width will be convoluted with the Lorentzian contribution of the isotope disorder whose width is predicted to be about one order of magnitude smaller (0.1 cm^{-1}). In such a case the disorder-induced lifetime would broaden the observed profile by about seven percent, an effect just at the edge of what might be detectable in our experiment. However, within the experimental error our data exhibit nearly the same profile widths for both samples. Possibly, the disorder-induced broadening was masked by a slight change of the slope of the dispersion due to the trivial harmonic mass shift. Simulations showed that this change of the slope may entail changes of the instrumental linewidth of the same size as that of the expected disorder effect and thus might enhance or cancel the disorder-induced broadening. As a result we have not been able to experimentally determine disorder-induced line broadenings for the acoustic branches.

In order to evaluate the positions of the phonon peaks we have fitted them with a superposition of two Gaussians that were constrained to approximately the same widths for both samples at a given energy transfer, and used the center of the Gaussian that describes the low $|\vec{q}|$ edge of the peak to define its position. The \vec{q} values were then converted into energies and corrected for the trivial mass dependence. As a result, the frequencies obtained for the disordered sample were up to 1 cm^{-1} higher than for the ordered one with the difference rising monotonically with $|\vec{q}|$ from zero at the lower end to the maximum value at the upper end of the investigated range. A similar behavior was observed in different energy ranges on the other branches. Consequently, we have obtained different energy shifts for phonons of similar energies

but with different propagation directions and polarizations. Both the magnitude and the frequency dependence of the observed effect are in conflict with the theoretical predictions and we suspect that they are due to systematic experimental errors hitherto not understood.

IV. THEORY

In an earlier publication, the isotope disorder in germanium was treated with the CPA as well as a SCBA. Surprisingly, the predictions of the two theories differed qualitatively from each other. Moreover, the SCBA results, but not the CPA results for Ge, are similar to those of recent CPA calculations for a similar system, i.e., isotopically disordered $\alpha\text{-Sn}$.¹⁵ This motivated us to repeat the CPA calculations for Ge, which indeed showed that earlier CPA results²⁰ contain numerical errors.

In addition to the CPA calculations, we thought it worthwhile to apply a fundamentally different approach to the problem of isotope disorder, i.e., by modeling our neutron-scattering experiments by means of SC's. This approach involves less approximations than the CPA and therefore can be expected to model the effects of isotope disorder more realistically provided the size of the unit cell of the SC is sufficiently large.

A. Coherent potential approximation

The CPA was developed in order to treat scattering in disordered systems in a coherent fashion.^{29,30} The basic idea is to let the periodic crystal potential be an unknown *complex* function, which one determines self-consistently in such a way that the average scattering produced by real scatterers embedded in the effective material is zero. Isotope disorder is a particularly simple case, since the force constants do not depend on the kind of atom located at a specific site (diagonal disorder), i.e., we assume that the lattice relaxation around isotope *impurities* has a negligible effect on the force constants. Therefore, one can check the validity of the CPA for materials that have a high degree of substitutional disorder but a small perturbing potential. In the single-site CPA one considers a fictitious crystal in which the masses are assumed to be complex and frequency dependent. One can write the CPA mass in terms of the dimensionless self-energy $\tilde{\epsilon}(\omega^2)$ as $m_{\text{CPA}} = \bar{m}[1 - \tilde{\epsilon}(\omega^2)]$. This self-energy is obtained self-consistently from the requirement that the average scattering vanishes, a condition that can be written as³¹

$$\tilde{\epsilon}(\omega^2) = \sum_i \frac{x_i r_i}{1 + [\tilde{\epsilon}(\omega^2) - r_i] \bar{m} \omega^2 G_0 \{ \omega^2 [1 - \tilde{\epsilon}(\omega^2)] \}}, \quad (1)$$

where x_i is the fraction of the isotope i and \bar{m} the average mass. The Green's function G_0 and the dimensionless mass deviations r_i are defined by

$$G_0(\omega^2) = \frac{1}{\bar{m}} \int \frac{\rho(\omega')}{\omega^2 - \omega'^2} d\omega', \quad r_i = \frac{\bar{m} - m_i}{\bar{m}}. \quad (2)$$

Here the one-phonon density of states ρ (DOS) of the ordered crystal is assumed to be normalized to 1. Equation (1) can be solved by iteration.

For the comparison of the CPA with SC results and with the experimental data, we need the spectral density function $A(\vec{q}, \omega)$ defined as the imaginary part of the \vec{q} -dependent phonon Green's function

$$A(\vec{q}, \omega) = \frac{1}{\pi} \text{Im} \left(\frac{2\omega(\vec{q})}{\omega^2 - \omega^2(\vec{q}) - 2\omega(\vec{q})\Pi(\vec{q}, \omega)} \right). \quad (3)$$

The phonon self-energy $\Pi(\vec{q}, \omega)$ is related to the reduced self-energy $\tilde{\epsilon}(\omega^2)$ used in the CPA formalism by

$$\Pi(\vec{q}, \omega) = \frac{1}{2} \frac{\omega^2}{\omega(\vec{q})} \tilde{\epsilon}(\omega^2). \quad (4)$$

For cubic symmetry²⁹ and if $\text{Im}[\Pi(\vec{q}, \omega)] \ll \omega(\vec{q})$ the spectral density function $A(\vec{q}, \omega)$ simplifies to

$$\begin{aligned} A(\vec{q}, \omega) &= \frac{1}{\pi} \text{Im} \left(\frac{1}{\omega - \omega(\vec{q}) - \Pi(\omega)} \right) \\ &= \frac{1}{\pi} \frac{\Gamma_{\text{CPA}}(\omega)}{[\omega - \omega(\vec{q}) - \Delta_{\text{CPA}}(\omega)]^2 + \Gamma_{\text{CPA}}^2(\omega)}, \end{aligned} \quad (5)$$

with $\Pi(\omega) = \frac{1}{2} \omega \tilde{\epsilon}(\omega^2)$. If the phonon density of states does not vary appreciably within the range of the main intensity of $A(\vec{q}, \omega)$, the quantities

$$\begin{aligned} \Delta_{\text{CPA}}(\omega) &= \frac{1}{2} \omega \text{Re}[\tilde{\epsilon}(\omega^2)], \quad \text{and} \\ \Gamma_{\text{CPA}}(\omega) &= -\frac{1}{2} \omega \text{Im}[\tilde{\epsilon}(\omega^2)]. \end{aligned} \quad (6)$$

describe the shift and width, respectively, of a phonon peak having a Lorentzian shape. In Sec. V we shall show that in Ge this applies well to the acoustic regime, whereas in the optical branches strong deviations from the symmetric Lorentzian shapes do occur. In this case it is no longer possible to characterize the spectral density function $A(\vec{q}, \omega)$ by just two parameters.

The phonon density of states of the disordered system $\rho_{\text{eff}}(\omega)$ is given by²⁹

$$\rho_{\text{eff}}(\omega) = \frac{2}{\pi\omega} \text{Im} \int \frac{\rho(\omega') \omega'^2}{\omega^2 [1 - \tilde{\epsilon}(\omega^2)] - \omega'^2} d\omega'. \quad (7)$$

In Fig. 5 we show the calculated real and imaginary part of the disorder-induced phonon self-energy in the acoustic and optical energy regime of Ge. These results prove that the oscillations seen in earlier CPA results are spurious.²⁰ In the optical regime, the real part $\Delta_{\text{CPA}}(\omega)$ changes from being negative (-1 cm^{-1}) at 280 cm^{-1} to being positive (2 cm^{-1}) at 295 cm^{-1} . The imaginary part $\Gamma_{\text{CPA}}(\omega)$ attains a maximum value of 2.2 cm^{-1} in the optical band. In the acoustic region ($\omega \leq 240 \text{ cm}^{-1}$) we find the self-energy effects to be about ten times smaller than in the optical region.

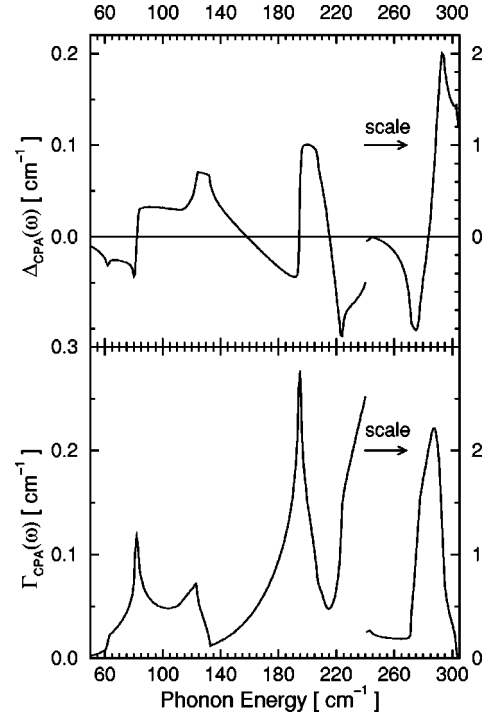


FIG. 5. Real and imaginary part of the disorder-induced phonon self-energy obtained from CPA calculations. We have used the VFM for the case of an isotopically disordered alloy having the same mass variance as our real sample ($^{70.15}\text{Ge}_{0.5}^{75.85}\text{Ge}_{0.5}$, $g = 1.52 \times 10^{-3}$). Note that the scales to the left and to the right differ by a factor of 10.

B. Supercell calculations

This approach is nonperturbative and exact within the assumptions made by using harmonic and phenomenological force constants as well as finite cell sizes. Assuming that isotope substitution leaves the lattice dynamical force constants unchanged, then the random filling of 50% of the lattice sites in a supercell with the lighter ^{70}Ge isotope and the occupation of the remaining sites with the heavier ^{76}Ge yields a perfect isotopic alloy. Using phenomenological models, like a valence force model (VFM) or the bond charge model³³ (BCM), to describe the lattice dynamics within the harmonic approximation, we obtain the eigenfrequencies and the eigenvectors through a diagonalization of the dynamical matrix of the supercells. This procedure yields the spectral density of states $D(\vec{q}, \omega)$, i.e., the distribution of the number of phonon states per frequency channel at a certain wave vector \vec{q} . In order to simulate the data obtained in an inelastic neutron scattering experiment, we weigh the spectral density of states $D(\vec{q}, \omega)$ with the dynamical structure factor σ of the respective mode, where σ is calculated from the momentum transfer and the eigenvectors obtained in the diagonalization.

Results obtained from the supercells of finite size depend on the particular mass configuration when filling the supercell with ^{70}Ge and ^{76}Ge atoms. In order to reduce the effects of the finite cell size, we averaged the spectra for several isotope configurations. Comparing the results for supercells of 64 and 216 atoms, respectively, and for different numbers of configurations, we came to the following conclusions: In the energy region of the optic branches, supercells of 64

atoms and about 30 isotope configurations are sufficient for our purposes, since larger supercells yield practically the same results. In the energy region of the acoustic branches, however, a large computational effort was necessary to arrive at reliable results, e.g., using supercells of 216 atoms or even more and many different configurations.

We checked in how far the calculated results for the projected spectral density of states $\sigma D(\vec{q}, \omega)$ depend on which of the equivalent crystallographic directions is chosen for \vec{q} and on the polarization of the phonon branch that is implicitly contained in σ . We found that the energy of the phonon under consideration seems to be the only relevant parameter, a result that is implicit in the CPA approach. We also checked to which extent the results depend on the underlying lattice dynamical model by using a VFM model and a bond charge model.³³ On average, both models give an equally good description of the data reported by Nilsson and Nelin,²⁴ but differ in detail as to how well particular phonon branches are described. Both models yield very similar results for the $\sigma D(\vec{q}, \omega)$ spectra; the differences can be largely understood on the basis of the slightly different description of the phonon dispersion and the resulting shapes of the DOS. The calculations presented in this paper are based on an extended valence force model with two angular forces and Born-von Kármán parameters reaching beyond the first-nearest neighbor.³² Compared to the commonly used BCM (Ref. 33) it gives a somewhat better reproduction of the optic branches, allows the use of larger supercells in our program and the calculations are much faster. Using our VFM the dynamical matrix of the supercells were explicitly constructed for each respective SC size and geometry. Unless specified differently, we used a cubic SC with $a_0 = 16.971 \text{ \AA}$ containing 216 atomic sites and 30 isotope configurations.

V. COMPARISON OF CPA AND SC

In order to compare the two different theoretical approaches that we have employed, we show examples of the spectral density function for the optical regime in Fig. 6(a). The full lines depict $A(\vec{q}, \omega)$ obtained in the CPA framework, while the symbols show the results of our supercell calculations. In both cases we have modeled the lattice dynamics with the VFM while the area underneath each curve has been normalized. Obviously, the spectral density functions obtained from these fundamentally different approaches agree extremely well with each other. The line shapes and positions are similar and the respective amplitudes are in agreement, so that from the inspection of $A(\vec{q}, \omega)$ we cannot discern a systematic difference between the two approaches, at least not for the mass disorder of our 70/76 sample ($g = 1.52 \times 10^{-3}$).

According to Fig. 5, the self-energy in the acoustic regime ($\omega \leq 240 \text{ cm}^{-1}$) is an order of magnitude smaller than those in the optical branches. Therefore, supercell calculations require the use of larger cells and averages over several phonons with the same energy in order to achieve results of sufficient accuracy in the acoustic regime. The most favorable condition is met in the vicinity of the peak in the DOS near 195 cm^{-1} . Calculations at this energy were carried out

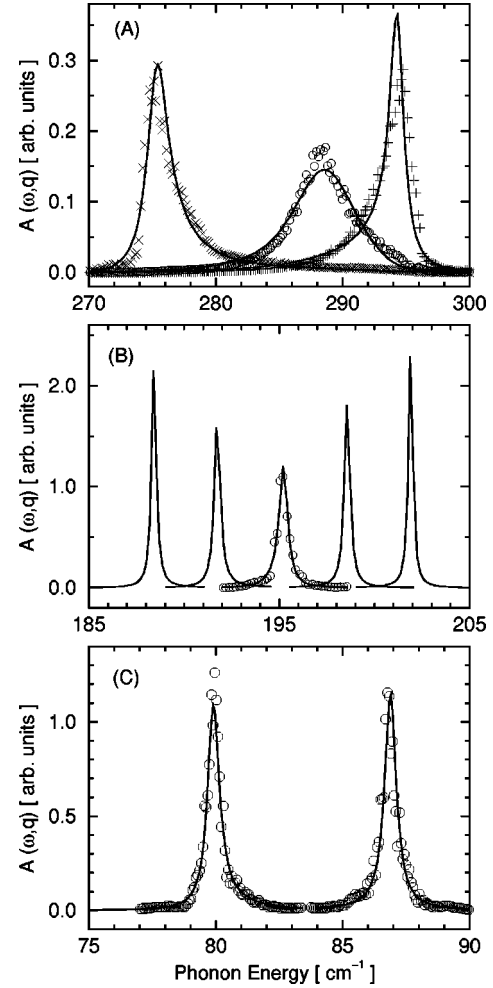


FIG. 6. Comparison of the spectral density functions obtained from supercell calculations (\times , \circ , $+$ symbols) and those obtained within the CPA framework (solid lines). (A) Calculated for $\omega(\vec{q}) = 276.5, 287.5,$ and 292.2 cm^{-1} and (B,C) spectra for a number of acoustic frequencies.

using an orthorhombic supercell of dimension $11.314 \times 16.971 \times 28.285 \text{ \AA}^3$ containing 240 atomic sites. This choice provides an improved sampling and allows the averaging over three equivalent phonons. In Fig. 6(b) we show the spectral density function $A(\vec{q}, \omega)$ calculated within the CPA in the acoustic regime as full lines and compare it to the result of the SC for $\omega(\vec{q}) = 195 \text{ cm}^{-1}$ shown as the \circ symbol. Both approaches agree well with each other. For even smaller frequencies the supercell results showed too much noise for a meaningful comparison. In order to allow a comparison between CPA and SC in the whole range of the experimental studies we have carried out calculations for a 67/79 isotopic alloy, again with the orthorhombic cell containing 240 sites. In these calculations we have studied LA phonons in the $\vec{q} = (\xi, 0, 0)$ and $(\xi, \xi, 0)$ directions at 80 cm^{-1} and 86.7 cm^{-1} , which lie below and above the prominent peak of the acoustic DOS. The results are shown in Fig. 6(c). We find that the phonon profiles are well approximated by Lorentzians but some asymmetry in the wings is clearly visible, both in the CPA and the SC results. From the good agreement between CPA and SC we infer that the CPA pro-

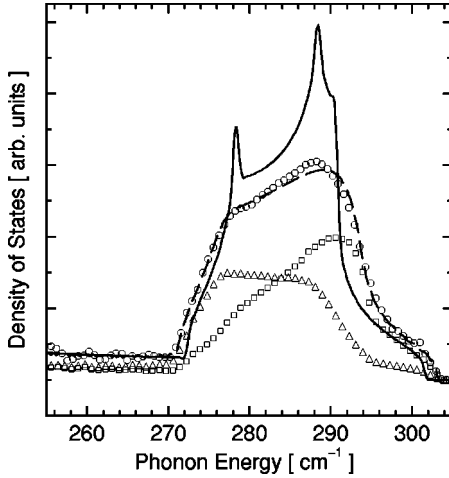


FIG. 7. The density of states in the region of the TO phonons obtained from our VFM model for the case of a perfect crystal (VCA) is depicted by the solid line. The \circ symbols display the DOS obtained from the SC, while the dashed line shows the DOS which results from the CPA. The projections of the SC DOS on the heavy and light masses are represented by the \triangle and \square symbols, respectively. Here, we used the root sampling method at about 1250 \vec{q} points in the irreducible part of the Brillouin zone to calculate the DOS of a tetragonal SC containing 96 atoms. The channel width is 0.16 cm^{-1} . The results shown are the average of 15 isotope configurations.

vides reliable results also for the low energy range of the 70/76 isotopic alloy.

As can be seen in Fig. 6(a), $A(\vec{q}, \omega)$ can exhibit strongly asymmetric line shapes. In fact, $A(\vec{q}, \omega)$ for $\omega(\vec{q}) = 276.5$ and 292.2 cm^{-1} show long tails towards the energy range of a higher DOS (compare Fig. 7). The most pronounced asymmetries occur when the unperturbed phonon frequency $\omega(\vec{q})$ lies in a region in which the real and imaginary part of the self-energy, Δ_{CPA} and Γ_{CPA} , respectively, vary strongly as a function of frequency. A constant Δ (Γ) can be directly interpreted as a shift (width) of a Lorentzian. However, from the asymmetric shapes of the peaks it is clear that this identification is not straightforward in those regions that encompass precipitous drops in the flanks of the phonon density of states.

We show the DOS $\rho(\omega)$ in the frequency range of the optical branches as the solid line in Fig. 7 obtained from our VFM for the case of a perfect crystal (VCA). Calculating the density of states for these two methods of treating disorder, we find some difference between the results of the two approaches: In Fig. 7 we show the DOS of the disordered system obtained from the SC and CPA as \circ symbols and a dashed line, respectively. We note that the small differences in the energy range from $282\text{--}294 \text{ cm}^{-1}$ become more pronounced for larger mass variances, for which the SC DOS starts to exhibit pronounced peaks, while the CPA DOS remains unstructured. For mass differences corresponding to Si-Ge alloys, we found that the SC DOS shows three rather sharp peaks, while the CPA DOS does not.

We have checked in how far the width of the isotope disorder-induced scattering, i.e., the width of $A(\vec{q}, \omega)$, depends on the size of the mass variance g in our supercell

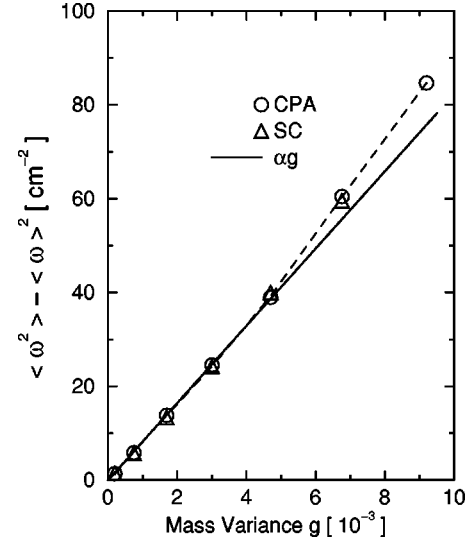


FIG. 8. Variance of the frequency of the spectral density function $A(\vec{q}, \omega)$ as a function of mass variance g calculated with the CPA (\circ) and the SC (\triangle). The solid line represents the proportionality to the mass variance g found for $g < 3 \times 10^{-3}$ extended to larger values of g .

calculations employing the VFM lattice dynamical model. The investigated supercells were 50/50 mixtures ranging from 73/73 to 67/79 isotopes, which corresponds to a mass variance of up to 6.755×10^{-3} . We have chosen the variance of the frequency $\langle \omega^2 \rangle - \langle \omega \rangle^2$ for the characterization of the width of the spectral density function, a quantity that is independent of the individual shape of $A(\vec{q}, \omega)$. This quantity is plotted in Fig. 8 versus the mass variance g for a phonon of $\omega(\vec{q}) = 276.5 \text{ cm}^{-1}$ with a strongly asymmetric line shape [see Fig. 6(a)] and is compared to the predictions of the CPA. We observe a deviation from linearity above $g = 3 \times 10^{-3}$ and excellent agreement between the results from CPA and SC in the whole range of the figure. Up to $g = 3 \times 10^{-3}$ good agreement is also found for the spectral density functions, whereas characteristic deviations show up beyond this value. This is demonstrated at the bottom of Fig. 9 where we find indications of a three peak structure in the SC results (marked by arrows) that are not well reproduced by the CPA. With increasing mass variances these structures become more pronounced and for very large values of g , they correlate with a three peak structure observed in Raman studies on Si-Ge alloys.³⁴ A more detailed discussion of this topic is beyond the scope of the present work.

We would like to note that the use of the terms *disorder-induced shift and broadening* could be misleading within the supercell approach. These expressions tend to be used in the framework of perturbational calculations, where they denote corrections due to phonon-phonon interactions, which are induced by the mass defects. In contrast, however, the dynamical matrices occurring in the framework of the supercell calculations can be diagonalized with a high precision. These calculations yield a manifold of phonon states $D(\vec{q}, \omega)$ having a zero width. In this approach the isotope disorder-induced broadening, which is clearly observed in Fig. 3(b), appears to be due to the scatter of the $3N$ eigenfrequencies (N is the number of atoms in the supercell), obtained for

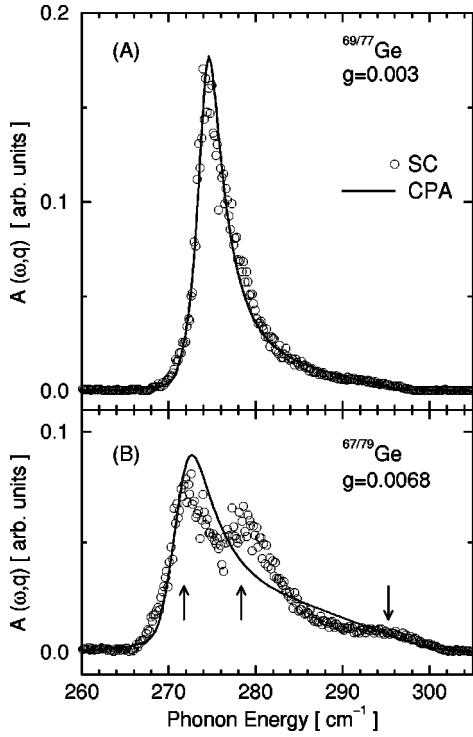


FIG. 9. Comparison of the spectral density function obtained from a SC with CPA results for $\omega(\vec{q})=276.5 \text{ cm}^{-1}$. (A) $^{69/77}\text{Ge}$, $g=3.002 \times 10^{-3}$, average of four phonons. (B) $^{67/79}\text{Ge}$, $g=6.755 \times 10^{-3}$, average of six phonons.

each isotope occupation of the supercell around the single frequencies of the respective branches obtained from the dynamical matrix in the VCA. Therefore, the width of the spectral density function $\sigma D(\vec{q}, \omega)$ obtained within the SC picture does not stem from a reduced lifetime resulting from disorder scattering (homogeneous broadening), but from a broad spectral density of discrete states that is ensemble averaged over many different isotope distributions. In the same way the shift does not occur in the sense of a corresponding real part of a self-energy but is determined by the exact shape of the spectral density function together with the particular experimental resolution.

VI. COMPARISON OF THEORY AND EXPERIMENT

When comparing our experimental results with theoretical predictions, we are confronted with the difficulty that the spectral density functions cannot be described by a universal function like a Gaussian or a Lorentzian and that the experimental resolution (“slit width”) is larger than the intrinsic widths of the spectral density functions. The latter effect tends to smear out details in the line shapes and will, in general, allow us to compare only integral quantities characterizing the width and the average frequency of a spectrum. In order to put the analysis on a common footing with the analysis of the experimental data, we proceeded as follows: We convoluted the spectral density functions obtained from either CPA or SC with a Gaussian profile whose width is given by the experimental resolution (compare Fig. 2). From a Gaussian fit of this result an excess width (broadening, $\delta\Gamma = \Gamma_{\text{fit}} - \Gamma_{\text{exp}}$) and a shift [$\delta\nu = \nu_{\text{fit}} - \nu(\vec{q})$] with respect to

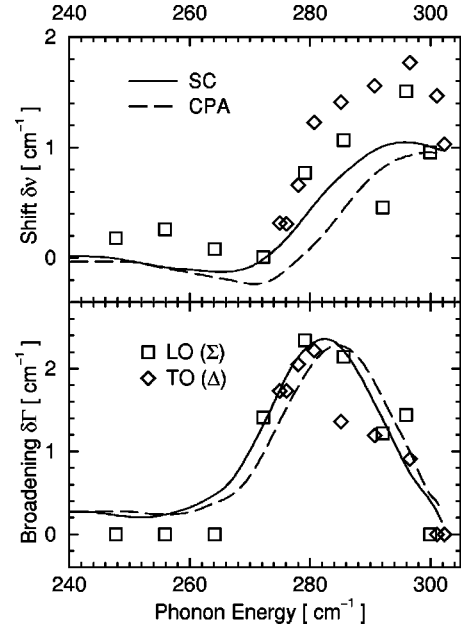


FIG. 10. Disorder-induced shift and broadening obtained from the convolution of the spectral density function with the Gaussian experimental resolution ($\Gamma_{\text{exp}}=11 \text{ cm}^{-1}$, FWHM). The solid line depicts the results of the supercell calculations and the dashed line those obtained within the CPA. In both cases we used the VFM for the lattice dynamics. The calculations were performed for the case of an isotopically disordered alloy having the same mass variance as our real sample ($^{70.15}\text{Ge}_{0.5}^{75.85}\text{Ge}_{0.5}$, $g=1.52 \times 10^{-3}$). The squares show the disorder-induced effects measured on the $\Sigma_3(O)$ branch, which has longitudinal character. The diamonds show those obtained on the $\Delta_5(O)$ branch, which has transverse character. The experimental errors in $\delta\nu$ and $\delta\Gamma$ are smaller than 0.4 cm^{-1} .

the VCA results were determined.

We have analyzed our experimental and theoretical results in the above manner and compare them in Fig. 10. We find good agreement between them for the excess width, whereby the supercell calculations reproduce the data points somewhat better. The agreement is not quite as good for the shift: The experimental points appear to lie systematically above the theoretical curves. Again, the supercell calculations seem to reproduce the data points better than the CPA. A further improvement can be obtained if we apply to the experimental data a constant frequency shift of about -0.3 cm^{-1} . Such a systematic error in the experimental data may arise from geometrical effects associated with the somewhat different shape of the samples or from uncertainties in their isotopic composition. Assuming that the disordered sample contained 1% more ^{70}Ge than listed in Table I and, consequently, that the crystal lacked 1% of ^{76}Ge we find that, within the virtual crystal approximation, its optical phonon frequencies should increase by about 0.15 cm^{-1} . Our experimental data for the two branches and two high symmetry directions in the optical region show no indication of a dependence of disorder-induced effects on the polarization nor on the particular reduced wave vector \vec{q} of the phonon, in agreement with the theoretical analysis.

The results of Fig. 10 are related to the real and imaginary parts of the disorder-induced self-energy displayed in Fig. 5. The convolution of the strongly asymmetric line profiles,

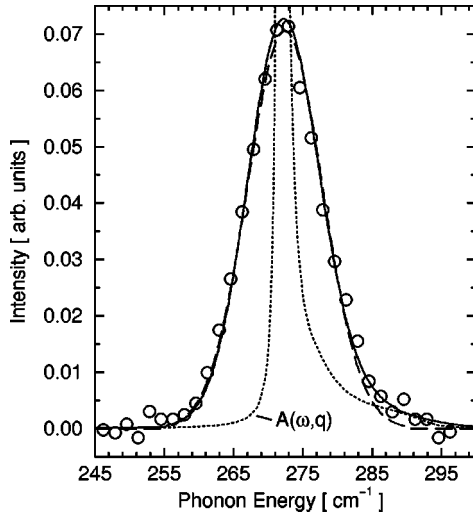


FIG. 11. The spectral density function $A(\vec{q}, \omega)$ calculated with the CPA for a phonon at the X point compared to the corresponding neutron results (\circ symbol). Dotted line: CPA result; solid line: after convolution with the experimental resolution [$\Gamma_{\text{exp}}=11.7 \text{ cm}^{-1}$, see Fig. 2(B)]; dashed line: fit of a Gaussian to the solid line.

which result from Eq. (5), with a Gaussian leads to a smearing of the structures and a reduction of the amplitudes of the curves plotted in Fig. 5. In particular, the pronounced negative real part in Fig. 5 near 275 cm^{-1} is strongly reduced.

Having shown that the experimental data and the theoretical predictions are in good agreement for quantities such as the average shift and broadening, we next consider the predicted asymmetry of the spectral density function. This asymmetry is resolved for the X point phonon spectra of the disordered $^{70/76}\text{Ge}$ sample with a rather good statistics. $A(\vec{q}, \omega)$ is shown in Fig. 11 as the narrow peak (dotted line) for $\omega(\vec{q})=274 \text{ cm}^{-1}$. The convolution of $A(\vec{q}, \omega)$ with the Gaussian spectrometer resolution yields the solid line in Fig. 11 ($\Gamma_{\text{exp}}=11.7 \text{ cm}^{-1}$, compare Fig. 2). It is clear from Fig. 11 that the properly convoluted spectral density function reproduces the small shoulder on the high-energy side of the X point spectrum rather convincingly. In contrast, a fit of a symmetric Gaussian (dashed line) describes the data less well. We have shifted the experimental data (\circ symbol) by 1.1 cm^{-1} since our VFM model was fitted to low-temperature neutron data.

VII. EARLIER RESULTS

A number of earlier publications deal with the isotope disorder effects in germanium.^{14,16,20,35,36} In particular, the energy dependence of the disorder-induced self-energy was investigated both theoretically and experimentally in Ref. 20. On the experimental side, Raman and neutron scattering, as well as infrared transmission and photoluminescence experiments, were carried out. On the theoretical side, calculations were performed using the CPA and the SCBA. Etchegoin *et al.* report that there is reasonably good agreement between theory and experiment for the CPA, whereas the SCBA was found not to reproduce the energy dependence of the disorder-induced shifts in the region $\sim 270\text{--}310 \text{ cm}^{-1}$.²⁰

From the present study and additional SCBA calculations we come to the conclusion that the theoretical results presented in Ref. 20 are incorrect. Especially, the $\text{Re}[\Sigma_{\text{CPA}}(\omega)]$ results of Figs. 3 and 9 of Ref. 20 in the region $\sim 270\text{--}310 \text{ cm}^{-1}$ are qualitatively in error, so that the preference given to the CPA over the SCBA in Ref. 20 must have been based on computational errors.

Comparing the experimental results presented in Fig. 9 of Ref. 20 to SC and CPA results calculated by us for natural Ge, we found good agreement between theory and experiment for the disorder-induced line broadening. Hereby, we note that our recalculated $\Gamma_{\text{CPA}}(\omega)$ does not differ strongly from those shown in Fig. 9 of Ref. 20. Regarding the shifts, we now understand why only small effects were seen in the earlier neutron experiments of a natural germanium crystal, since our present simulations yield shifts $\Delta_{\text{CPA}}(\omega)$ that are about three times smaller than those expected from the theoretical results of Ref. 20. At the Γ point, the shift observed by neutrons was about two times smaller than the Raman value of Ref. 20. However, the small Γ point shift was confirmed by the most recent data¹⁶ obtained from our $^{70/76}\text{Ge}$ sample using Raman scattering at 10 K. A disorder-induced shift of $\delta\nu = +1.06(4) \text{ cm}^{-1}$ was found that compares favorably with our present neutron result and reflects the high accuracy achieved in the neutron measurements. With hindsight, it was practically hopeless to extract shifts from the former neutron data for natural germanium with sufficient accuracy to test different theories. As for the shifts deduced from optical experiments, we found that the photoluminescence data are in reasonable agreement with theory. The values evaluated from IR transmittance, however, show a behavior that is not consistent with the present theories. In conclusion, not too much can be learned from the previous data of Ref. 20, mainly because the disorder-induced effects are so small in natural Ge.

In Ref. 36 Fuchs and co-workers report additional very low-intensity features between 270 and 295 cm^{-1} in the Raman spectra of isotopically disordered germanium, so-called band modes. Similar results were obtained in α tin.¹⁵ In Fig. 4 of Ref. 36, the experimental results are compared to calculations of incoherent scattering based on earlier CPA calculations, which clearly cannot account for the data, since the latter predict a vanishing intensity around $\sim 282 \text{ cm}^{-1}$. Earlier calculations of the coherent scattering intensity of the band modes yielded negligible intensities and thus were not presented in Ref. 36. Our present CPA results improve the situation.

In Fig. 12 we show the Raman signal stemming from the disorder-induced band modes together with the CPA calculation from Ref. 36 as the solid and dotted lines, respectively. The Raman intensity was obtained by subtracting a symmetric Lorentzian that represented the Raman signal of an isotopically pure sample from that of an isotopically disordered $^{70}\text{Ge}_{0.5}^{76}\text{Ge}_{0.5}$ sample (compare Fig. 2 in Ref. 36). Here, it needs to be pointed out that the finite resolution of the DILOR Raman spectrometer used in Ref. 36 was neglected in the analysis. We have checked that a Gaussian resolution between 0 cm^{-1} (ideal case) and 2.5 cm^{-1} , that corresponds to the typical resolution of this DILOR spectrometer, changes the amplitude of the band modes in $^{70/76}\text{Ge}$ from ~ 0.002 to ~ 0.012 , when the maximum of the main line is

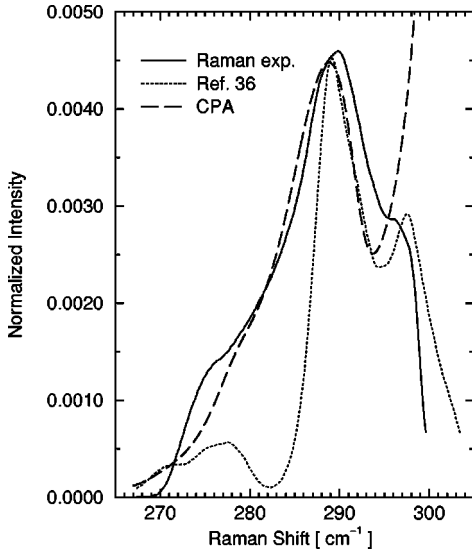


FIG. 12. Comparison of our CPA results with earlier Raman experiments and CPA calculations by Fuchs *et al.* The intensity scale is obtained by setting the maximum of the main Raman line to one. The solid and dotted lines are reproduced from Fig. 4 of Ref. 36 and represent the Raman signal of disorder-induced band modes in $^{70}\text{Ge}_{0.5}^{76}\text{Ge}_{0.5}$ and their CPA calculation, respectively. The dashed line depicts our CPA simulation of the Raman band mode signal [$\omega(\vec{q}) = 302.2 \text{ cm}^{-1}$]. Its intensity was divided by a factor of 2.

normalized to one. Furthermore, the subtraction of the main Raman line (without having it convoluted with the spectral resolution) results in additional uncertainties which render the band mode intensity above $\sim 294 \text{ cm}^{-1}$ unreliable. Therefore, we cannot reconstruct the absolute band mode intensity and can only make a qualitative comparison. Despite these quantitative uncertainties we find a very good qualitative agreement of our new CPA results with the Raman data between 270 and 294 cm^{-1} in the following way: From Eq. (3) and using Eq. (6), i.e.,

$$\Pi(\omega) = \frac{1}{2}\omega \text{Re}[\tilde{\epsilon}(\omega^2)] + i \left\{ -\frac{1}{2}\omega \text{Im}[\tilde{\epsilon}(\omega^2)] + 0.3 \text{ cm}^{-1} \right\},$$

we obtain the spectral density function $A(\vec{q}, \omega)$. The 0.3 cm^{-1} in the imaginary part of $\Pi(\omega)$ represent a frequency-independent anharmonic broadening and correspond to the 0.6 cm^{-1} FWHM of an isotopically pure Ge crystal at low temperatures.¹⁶ To account for the spectrometer resolution we convoluted $A(\vec{q}, \omega)$ with a Gaussian of 2.0 cm^{-1} FWHM. Then we subtracted the convolution of a Lorentzian (0.6 cm^{-1} FWHM) with a Gaussian (2.0 cm^{-1} FWHM), i.e., the simulation of the symmetric optical zone center phonon obtained in an ordered crystal. The result is shown as the dashed line in Fig. 12 after it was divided by two. This adjustment reflects the uncertainty in reconstructing the absolute intensity of the band modes. Comparing the dashed line with the Raman line we conclude that the proper CPA calculation of the coherent scattering intensity together with the experimental resolution effects are able to predict the frequency dependence of the band mode intensity and

that the strong intensity of the incoherent scattering presented in Ref. 36 might have arisen from the numerical problems of Ref. 20.

From Refs. 22 it is expected that the disorder-induced broadening $\delta\Gamma$ should be proportional to the one-phonon density of states [$\delta\Gamma \sim \tau^{-1} \sim g\omega^2\rho(\omega)$]. However, the SC calculations of $\delta\Gamma$ for optical phonons having different wave vectors, polarizations, and frequencies deviate by as much as a factor of 2 from this relation, revealing that the above formula, based on second order perturbation theory, is only a crude approximation that neglects the potential asymmetry of $A(\vec{q}, \omega)$.

VIII. CONCLUSION

We have presented a comprehensive study of the influence of isotope disorder on the phonons in Ge by means of inelastic neutron scattering and corresponding lattice dynamical calculations using either the CPA or supercells (SC). Germanium is particularly well suited for such a study due to the existence of stable isotopes with differences of up to 9% in their atomic masses and a strongly peaked phonon density of states in the optical region of TO phonons, exhibiting steep flanks on both sides of the peak, its rather harmonic lattice potential, and an excellent knowledge of its phonon dispersion relation. We have used the CPA and SC approaches to calculate $A(\vec{q}, \omega)$ for a sample containing a 50/50 mixture of the ^{70}Ge and ^{76}Ge isotopes. In the acoustic regime the resulting disorder leads to symmetric profiles and the shifts and widths are determined by the real and imaginary parts of the phonon self-energy. In the optical branches the steep flanks in the phonon density of states lead to pronounced asymmetries in the spectral density functions which are observed in the phonon scans. These asymmetries of $A(\vec{q}, \omega)$ are reproduced by the CPA as well as by the SC calculations and the association of the real and imaginary part of the self-energy with a shift and broadening, respectively, does not longer hold. Experiment and SC results further confirm the assumption of the single-site CPA that in a cubic structure the phonon profiles do not depend on the direction of propagation nor on the polarization of the phonon. Our analysis demonstrates that for this composition, i.e., this particular mass variance, the CPA accounts very well for the isotope disorder effects in the phonon profiles. The present CPA calculation improves previous results of Ref. 20 that probably suffered from convergence problems in the iteration process.

When comparing the results of the theoretical approaches to the experimental data, we find that, within the experimental uncertainty, the latter are well described by both theoretical methods. However, we find small, albeit systematic, differences between the shifts and broadenings obtained from the two calculations. Moreover, the experimental data for the disorder-induced shift seem to be better reproduced by the SC approach rather than the CPA. Further evidence for possible limitations of the elegant CPA are differences in the DOS calculated for the disordered solid when compared to SC results. Furthermore, for larger differences in the isotope masses characteristic structures in the spectral density functions of optical phonons are calculated within the SC approach, which are not well reproduced by the CPA, although

for an average quantity such as the variance of the frequency the agreement between CPA and SC is still perfect. Based on this work we cannot predict if similar results are to be expected for all systems. It might be that the shortcomings of the CPA are particularly pronounced in the case of Ge because of the low coordination number in the diamond structure and the extreme dominance of the first-neighbor interaction. Because of the low coordination number there will be many clusters where one light (heavy) atom is surrounded by light (heavy) atoms only and because of the short range of the atomic interactions in germanium the vibrational spectrum of the central atom of such clusters will closely resemble that of a solid consisting of light (heavy) atoms only. This situation will not be properly described by the standard

CPA, a limitation that might be resolved when using a CPA that is extended to clusters, as proposed in Refs. 37–40.

ACKNOWLEDGMENTS

We are indebted to K. Kunc for a critical reading of the manuscript. A.G. gratefully acknowledges stimulating discussions with Bert Koopmans and Thomas Strohm. Thanks are due to V. I. Ozhogin, at the Kurchatov Institute, for the isotopic separation, and A. Schmeding for an accurate determination of the isotopic composition of the alloyed sample. This work was supported in part by the US NSF through Grant No. DMR-94 17763 and in part by the Director, Office of Energy Research, Office of Basic Energy Sciences, Division of Materials Sciences, of the U.S. Department of Energy under Contract No. DE-AC03-76SF00098.

*Present address: Keio University, 3-14-1 Hiyoshi, Kohokuku, Yokohama 223, Japan.

¹M. Cardona, in *Festkörperprobleme/Advances in Solid State Physics*, Vol. 34, edited by R. Helbig (Vieweg, Braunschweig/Wiesbaden, 1994), p. 35.

²A. K. Ramdas, *Solid State Commun.* **96**, 111 (1995).

³E. E. Haller, *J. Appl. Phys.* **77**, 2857 (1995).

⁴T. Ruf, H. D. Fuchs, and M. Cardona, *Phys. Bl.* **52**, 1115 (1996).

⁵R. C. Buschert, A. E. Merlini, S. Pace, S. Rodriguez, and M. H. Grimsditch, *Phys. Rev. B* **38**, 5219 (1988).

⁶P. Pavone and S. Baroni, *Solid State Commun.* **90**, 295 (1994).

⁷J. C. Noya, C. P. Herrero, and R. Ramírez, *Phys. Rev. B* **56**, 237 (1997).

⁸A. Debernardi and M. Cardona, *Phys. Rev. B* **54**, 11 305 (1996).

⁹N. Garro, A. Cantarero, M. Cardona, A. Göbel, T. Ruf, and K. Eberl, *Phys. Rev. B* **54**, 4732 (1996); A. Göbel, T. Ruf, M. Cardona, C. T. Lin, J. Wrzesinski, M. Steube, K. Reimann, J.-C. Merle, and M. Joucla, *ibid.* **57**, 15 183 (1998).

¹⁰S. Zollner, M. Cardona, and S. Gopalan, *Phys. Rev. B* **45**, 3376 (1992).

¹¹C. Parks, A. K. Ramdas, S. Rodriguez, K. M. Itoh, and E. E. Haller, *Phys. Rev. B* **49**, 14 244 (1994).

¹²D. Rönnow, L. F. Lastras-Martínez, and M. Cardona, *Eur. Phys. J. B* (to be published).

¹³M. Asen-Palmer, K. Bartkowski, E. Gmelin, M. Cardona, A. P. Zhernov, A. V. Inyushkin, A. Taldenkov, V. I. Ozhogin, K. M. Itoh, and E. E. Haller, *Phys. Rev. B* **56**, 9431 (1997); W. S. Capinski, H. J. Maris, E. Bauser, I. Silier, M. Asen-Palmer, T. Ruf, M. Cardona, and E. Gmelin, *Appl. Phys. Lett.* **71**, 2109 (1997).

¹⁴H. D. Fuchs, C. H. Grein, R. I. Devlen, J. Kuhl, and M. Cardona, *Phys. Rev. B* **44**, 8633 (1991).

¹⁵D. T. Wang, A. Göbel, J. Zegenhagen, and M. Cardona, *Phys. Rev. B* **56**, 13 167 (1997).

¹⁶J. M. Zhang, M. Giehler, A. Göbel, T. Ruf, M. Cardona, E. E. Haller, and K. Itoh, *Phys. Rev. B* **57**, 1348 (1998).

¹⁷A. Göbel, T. Ruf, C.-T. Lin, M. Cardona, J.-C. Merle, and M. Joucla, *Phys. Rev. B* **56**, 210 (1997).

¹⁸Lei Wang, J. A. Wolk, L. Hsu, E. E. Haller, J. W. Erickson, M. Cardona, T. Ruf, J. P. Silveira, and F. Briones, *Appl. Phys. Lett.*

70, 1831 (1997); and references therein.

¹⁹This holds for Si, Ge, and α tin, while diamond is a notable exception.

²⁰P. Etchegoin, H. D. Fuchs, J. Weber, M. Cardona, L. Pintschovius, N. Pyka, K. Itoh, and E. E. Haller, *Phys. Rev. B* **48**, 12 661 (1993).

²¹L. Pintschovius, *Nucl. Instrum. Methods Phys. Res. A* **338**, 136 (1994).

²²S.-I. Tamura, *Phys. Rev. B* **27**, 858 (1983); H. J. Maris, *ibid.* **41**, 9736 (1990).

²³G. Nelin and G. Nilsson, *Phys. Rev. B* **5**, 3151 (1972).

²⁴G. Nilsson and G. Nelin, *Phys. Rev. B* **3**, 364 (1971).

²⁵J. Kulda and J. Saroun, *Nucl. Instrum. Methods Phys. Res. A* **379**, 155 (1996).

²⁶J. Menéndez and M. Cardona, *Phys. Rev. B* **29**, 2051 (1984).

²⁷D. W. Posener, *Aust. J. Phys.* **12**, 184 (1959).

²⁸J. Saroun and J. Kulda, *Physica B* **234-236**, 1102 (1997).

²⁹D. W. Taylor, *Phys. Rev.* **156**, 1017 (1967).

³⁰P. Soven, *Phys. Rev.* **156**, 809 (1967).

³¹E. Economou, in *Green's Functions in Quantum Physics*, 2nd ed., edited by P. Fulde (Springer, Berlin, 1983).

³²W. Reichardt (unpublished).

³³W. Weber, *Phys. Rev. B* **15**, 4789 (1977).

³⁴C. H. Grein and M. Cardona, *Phys. Rev. B* **45**, 8328 (1992); S. de Gironcoli and S. Baroni, *Phys. Rev. Lett.* **69**, 1959 (1992); H. Rücker and M. Methfessel, *Phys. Rev. B* **52**, 11 059 (1995); H. Rücker, M. Methfessel, B. Dietrich, K. Pressel, and H. J. Osten, *ibid.* **53**, 1302 (1996).

³⁵H. D. Fuchs, C. H. Grein, M. Bauer, and M. Cardona, *Phys. Rev. B* **45**, 4065 (1992).

³⁶H. D. Fuchs, P. Etchegoin, M. Cardona, K. Itoh, and E. E. Haller, *Phys. Rev. Lett.* **70**, 1715 (1993).

³⁷F. Yonezawa and T. Odagaki, *Solid State Commun.* **27**, 1199 (1977); **27**, 1203 (1977).

³⁸F. Yonezawa, in *The Structure and Properties of Matter*, edited by T. Matsubara, Springer Series in Solid State Sciences Vol. 28 (Springer, Berlin, 1982).

³⁹R. J. Elliott, J. A. Krummhanl, and P. L. Leath, *Rev. Mod. Phys.* **46**, 465 (1974).

⁴⁰P. N. Sen and W. M. Hartmann, *Phys. Rev. B* **9**, 367 (1974).